Electronic Journal of Biotechnology 66 (2023) 84–91

Contents lists available at ScienceDirect

Electronic Journal of Biotechnology

journal homepage: www.elsevier.com/locate/ejbt

Short Communication

Screening microbially produced pentyl diacetic acid lactone using an *Escherichia coli* biosensor workflow

Meng Gao [a,b,1], Yue Zhang [b,1], Lei Xue [b], Jie Li [b], Zhe Zhou [b], Xiaodan Li [b], Zhengxiong Zhou [b,c,*], Ren Wang [a,b,*]

[a] Nanjing University of Chinese Medicine, Nanjing 210023, China
[b] Jiangsu Key Laboratory for the Research and Utilization of Plant Resources, Institute of Botany, Jiangsu Province and Chinese Academy of Sciences, Nanjing 210014, China
[c] The Key Laboratory of Industrial Biotechnology, Ministry of Education, School of Biotechnology, Jiangnan University, Wuxi 214122, China

GRAPHICAL ABSTRACT

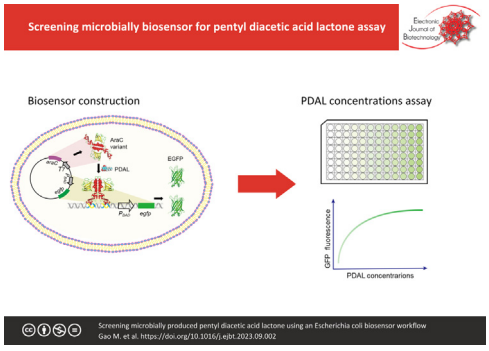

ARTICLE INFO

Article history:
Received 26 March 2023
Accepted 8 September 2023
Available online 4 October 2023

Keywords:
Biosensor
Cannabinoids
Escherichia coli
Olivetolic acid
Pentyl diacetic acid lactone
Prescription drugs
Rational design
Tetraketide synthase

ABSTRACT

Background: Cannabinoid compounds have been approved as prescription drugs for treating various human ailments. However, the production using both microbial and plant-based sources is time-consuming and expensive because their yield is extremely low. Tetraketide synthase (TKS), the key enzyme in the biosynthesis of cannabinoid compounds, produces only 4% of the intermediate compound olivetolic acid. However, it may be possible to rearrange the carbon metabolic flux of TKS using genetic methods to increase the overall yields of cannabinoid compounds. In this context, protein engineering is an economically beneficial and viable solution to improve the catalytic activity of TKS. However, the ability to produce enzyme variants significantly exceeds the capacity to screen and identify high producers, creating a bottleneck in the enzyme engineering process.
Results: This study constructed an *Escherichia coli*-based biosensor workflow for detecting the byproduct pentyl diacetic acid lactone (PDAL). Rational design was used to generate *E. coli* strains with mutant regulatory protein AraC and an altered effector PDAL to control the transcription of *gfp* and kanamycin. The developed biosensor could detect PDAL at the concentrations of the operational range from microbial cell culture and cell-free catalytic system.
Conclusions: The *E. coli*-based biosensor developed in this study efficiently detected PDAL with high throughput and low cost.

Peer review under responsibility of Pontificia Universidad Católica de Valparaíso
* Corresponding authors.
E-mail addresses: zhouzhx86@gmail.com (Z. Zhou), rwang@cnbg.net (R. Wang).
[1] These authors contributed equally to this study.

https://doi.org/10.1016/j.ejbt.2023.09.002

How to cite: Gao M, Zhang Y, Xue L, et al. Screening microbially produced pentyl diacetic acid lactone using an *Escherichia coli* biosensor workflow. Electron J Biotechnol 2023;66. https://doi.org/10.1016/j.ejbt.2023.09.002.

1. Introduction

Botanical polyketide synthases (PKSs, type III) are homodimeric enzymatic machines that biosynthesize structurally and functionally diverse natural compounds. These compounds are widely used as antibiotics (caprazamycins [1], acridones, xanthones, stilbenes, and anthraquionones), antimalarial agents (acridones), antioxidants (isoflavones and flavones), antiparasitic drugs (aurones), cardioprotective agents (stilbenes), immunosuppressants, antiplatelet aggregation drugs (phenanthrene), and cancer chemotherapy medications (aurones and isoflavones) [2]. Mechanistically different from the other two subgroups of PKSs, type III PKSs are structurally simpler and do not have multidomain [3,4] and multienzyme complexes [5,6]. Their biosynthesis is initiated via the Claisen condensation of thioesters to assemble a functionalized linear chain [7]. The products of PKSs are subsequently catalyzed by cyclase for benzene ring formation. However, metabolic flux imbalance and low biosynthetic efficiency lead to low productivities, titers, and product yields, making the catalytic step of PKSs a major bottleneck in polyketide biosynthesis. Moreover, to date, the mechanism of the biocatalytic system of natural PKSs remains unclear [8]. To better understand how PKSs synthesize these compounds, X-ray, nuclear magnetic resonance crystal structure, and computational analyses have been used to provide insights into the molecular basis of the catalysis process [9]. Based on these analyses, protein engineering, including domain exchange [10,11] and motif swapping [12], has been utilized to enhance biocatalytic efficiency or alter product distribution to improve the target compound production [13].

Cannabinoids are important polyketides, and >125 different cannabinoids have been isolated and identified from plants [14]. These compounds can bind to one or more receptors of the endocannabinoid system and regulate numerous physiological and pathological processes [15]. Cannabinoids have been used in the form of multitarget antitumor therapy agents [16,17,18] and nutraceuticals. They can improve the quality of life of patients with cancer because of their different supportive effects [19]. The biosynthetic pathway of cannabinoid production begins with the interactive condensation of malonyl-CoA and hexanoyl-CoA, catalyzed by tetraketide synthase (TKS), into a linear tetraketide intermediate. The intermediate is subsequently catalyzed by olivetolic acid cyclase to form olivetolic acid. However, the yield of olivetolic acid from malonyl-CoA and hexanoyl-CoA is <4%, which limits the biosynthesis of cannabinoids (Fig. 1). To address this issue, a novel method is needed to change the enzymatic functions of TKS using protein engineering. This modification may limit the diffusion of transient intermediates, prevent crosstalk between competitive metabolic pathways, and minimize the degradation or loss of unstable intermediates, thereby increasing the overall yield of olivetolic acid [10]. From this perspective, various methodological approaches are required to change the catalytic machinery or catalytic activity of TKS. However, testing the products and byproducts of TKS is more difficult than building an enzyme mutant, which creates obstacles in the protein engineering development cycle. Methods used for quantifying the tetraketide intermediates pentyl diacetic acid lactone (PDAL), hexanoyl triacetic acid lactone (HTAL), and olivetol (such as liquid chromatography–mass spectrometry [LC–MS]) are tedious, time-consuming, expensive, and lack the required throughput in terms of equipment and expertise. Thus, a cheap and powerful tool is needed for the detection and quantification of these metabolites. Biosensors are analytical devices that are extensively employed in many fields [20], including process control [21], fermentation analysis [22], pollution monitoring [23,24], and viral analysis [25,26]. Therefore, biosensors have been proposed as an alternative to resolve the aforementioned bottleneck.

AraC is a regulatory protein in *Escherichia coli* that regulates gene transcription via the *ara* operon. AraC represses gene transcription in the absence of $_{L}$-arabinose and activates it when $_{L}$-arabinose is present. This type of regulatory mechanism has been well-studied in several applications. In previous studies, the AraC effector was engineered to respond to mevalonate [27], triacetic acid lactone [28], and $_{D}$-arabinose [29].

The present study developed a new AraC mutant-based biosensor that was sensitive to a range of PDALs. Using this *E. coli*-based biosensor, the study demonstrated the detection of microbially produced PDAL. As a living sensor, it served as a tool for measuring the relative production yields of a library of TKS mutants.

2. Materials and methods

2.1. Strains, plasmids, cultures, and chemicals

All strains and plasmids used in the present study are listed in Table S1. *E. coli* BL21 was used as the host for gene cloning and expression. For expression in *E. coli*, the codon-optimized *Cannabis sativa TKS* gene was synthesized using Genscript (Nanjing, Jiangsu, China) and incorporated into pCold after digestion with *Nde*I and *Xba*I to generate pCold-*TKS*. The AraC protein-encoding gene *araC* from *E. coli* was amplified using primers F1/R1 and inserted into pET20b (+) after digestion with *Nde*I and *Hin*dⅢ to produce pET20b (+)-*araC*. The BAD promoter and *Kana* or *gfp* were amplified using F2/R2 and F3/R3 or F4/R4, respectively (Table S2), and fused via a one-step assembly to generate P_{BAD}-*Kana* or P_{BAD}-*gfp*. They were then inserted into pET20b (+)-*araC* to generate pET20b (+)-*araC*-P_{BAD}-*Kana* and pET20b (+)-*araC*-P_{BAD}-*gfp*, respectively. The Luria–Bertani (LB) medium (peptone 5 g/L, yeast extract 10 g/L, and NaCl 10 g/L) was used in all DNA manipulations and protein overexpression experiments. When necessary, 50 μg/mL ampicillin or 20 μg/mL kanamycin was added to exert selective pressure, 0.1 mM isopropyl-β-D-thiogalactopyranoside (IPTG) was added to induce *araC* expression, and 0.01–1 mM PDAL was added to regulate *Kana* and *gfp* expression. PDAL was synthesized in our laboratory (Fig. S1), whereas all other high-grade chemicals were obtained commercially.

2.2. Mutation of PDAL-binding AraC pocket

Based on the structure of *E. coli* AraC (PDB: 2ARC), the sizes of the substrate-binding pockets were calculated using CASTP (https://cast.engr.uic.edu/cast/) and POVME software [30]. The partially flexible CDOCKER software was used to perform docking between AraC and PDAL. The conformations of the ligand PDAL were generated based on high-temperature dynamics. Simulated annealing was utilized to optimize the flexible ligand conformation

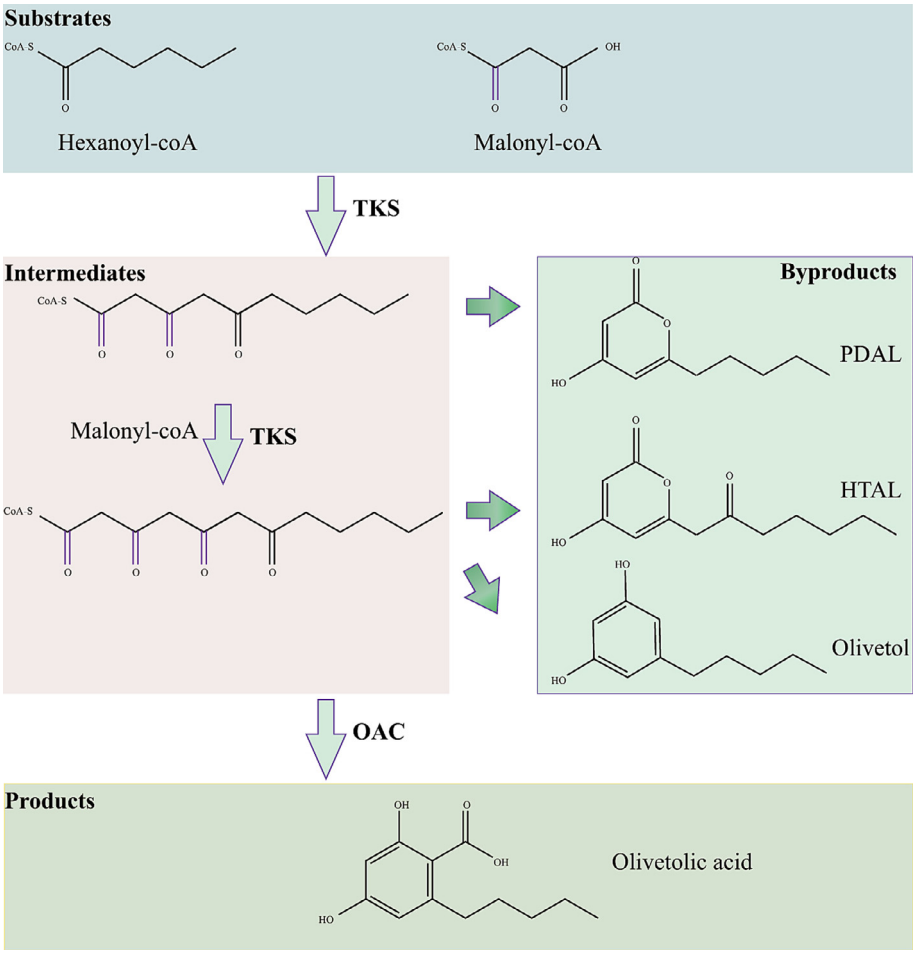

Fig. 1. Type III PKS gene of olivetolic acid biosynthesis in plants.

at the AraC binding pocket site. For this process, the default parameter was set to retain the first 10 conformations of the optimal ligand. The binding AraC sphere was generated using a radius of 10 Å. The optimal docking poses were obtained for subsequent analysis based on the highest standard of the CDOCKER Energy score (Table S3). To explore the key amino acid residues in the AraC pocket site, alanine scanning was performed using the Calculate Mutation Energy (Binding) module of the Discovery Studio 2017 software (Accelrys, Omaha, NE, USA). Mutation energies >0.5 kcal/mol or <−0.5 kcal/mol were selected for saturation mutation, and single-point mutants with the mutation energies of <−0.5 kcal/mol were chosen as the optimal site mutations. The structural diagrams were generated using PyMOL 1.8 (https://pymol.sourceforge.net).

2.3. Growth-based positive and negative screening

Screening was performed as described in a previous study with minor modifications [31]. In brief, after the plasmid pET20b (+)-*araC*-P_{BAD}-*Kana* and its mutant were transformed into *E. coli* BL21 to generate *E. coli* BL21 pET20b (+)-*araC*-P_{BAD}-*Kana* and its mutant, the strains were cultured in LB medium with 50 μg/mL ampicillin at 37°C for 12 h. They were then transferred to fresh LB medium with 50 μg/mL ampicillin and 0.1 mM IPTG to induce *araC* expression. After 2 h, 20 μg/mL kanamycin was added to the broth, 0.1 mM PDAL was added for positive screening, and DMSO was added to the control.

2.4. PDAL concentration during strain growth

PDAL concentration was assayed at different time points during *E. coli* BL21 pET20b (+) growth. In brief, the strain was cultured in LB medium with 50 μg/mL ampicillin and 0.1 mM PDAL at 37°C for 12 h. The culture supernatant was collected for PDAL concentration assay.

2.5. GFP expression fluorescence assays

Fluorescence assays were performed as previously described [32]. In brief, *E. coli* BL21 harboring the plasmid pET20b (+)-*araC*-P_{BAD}-*gfp* or its mutants were cultured overnight in LB medium containing 50 μg/mL ampicillin. They were then transferred to fresh LB medium with 50 μg/mL ampicillin and 0.1 mM IPTG to induce *araC* expression. After 2 h, 0.01–1 mM PDAL was added to the medium. After culture at 37°C for 12 h, the cells were collected and washed with Tris-HCl buffer solution (pH 7.4). The cell suspension was then diluted to OD_{600} = 0.5, and the fluorescence emission was measured using a multidetection microplate reader (Synergy 4, BioTek, VT, USA) via 488-nm excitation and 520-nm emission filters.

2.6. TKS purification

For TKS purification, *E. coli* BL21 pCold-*TKS* was cultured overnight, inoculated at a ratio of 1% (v/v) into fresh LB broth,

and incubated at 37°C with 220-rpm shaking for 2 h. Next, 100 μM IPTG was added to induce *TKS* expression. After incubation for 24 h at 16°C, the cells were collected by centrifugation at 10,000 × *g* and 4°C for 5 min and then resuspended in 10 mM Tris-HCl buffer (pH 7.4). The cells were subsequently disrupted via sonication, and the supernatant obtained by centrifugation at 12,000 × *g* and 4°C for 30 min was filtered through a 0.22-μm membrane for TKS purification. The TKS-containing filtrate was purified with Ni-NTA agarose using affinity chromatography (GE Healthcare, Little Chalfont, UK). In brief, Ni-NTA agarose was incubated with the filtered supernatant and washed thoroughly with the washing buffer (10 mM Tris-HCl, 30 mM imidazole, and 500 mM NaCl; pH 7.4). TKS was released from Ni-NTA agarose using the elution buffer (10 mM Tris-HCl, 300 mM imidazole, and 500 mM NaCl; pH 7.4). The concentration of the purified TKS was determined using a modified Bradford protein assay kit (Sango, Shanghai, China) with bovine serum albumin as the standard. TKS concentration was adjusted to 10 g/L in 10 mM Tris-HCl (pH 7.4) and stored for enzymatic assays.

2.7. In vitro PDAL assays

In vitro catalytic TKS activity was assayed to detect the product yield of PDAL, hexanoyl triacetic acid lactone, olivetol, and olivetolic acid [33]. A standard TKS reaction mixture comprising 5 mM 1,4-dithiothreitol, 0.2 mM hexanoyl-CoA, 0.6 mM malonyl-CoA, and 2.5 mM $MgCl_2$ in 20 mM HEPES (pH 7.4) buffer was incubated at 10°C for 24 h, and 1 mL of the resulting products was added into LB medium to determine GFP expression using the multidetection microplate reader.

2.8. In vivo PDAL assay

In vivo PDAL concentration was determined using fluorescence assays that assessed its correlation with the formation of free GFP. In brief, a single colony of *E. coli* BL21 harboring pCold-*TKS* and pET20b (+)-*araC*-P_{BAD}-*gfp* was cultured overnight in 3 mL LB medium with 50 μg/mL ampicillin. The culture was then incubated in 50 mL LB medium with 50 μg/mL ampicillin at 37°C for 2 h. Then, 0.1 mM IPTG and 0.01–1 mM PDAL were added to the medium to induce *gfp* expression at 16°C for another 24 h. Finally, 1 mL of the resulting culture was centrifuged, and the cells were washed with 10 mM Tris-HCl (pH 7.4) buffer and resuspended in 1 mL of the same buffer. The cultures were diluted to OD_{600} = 1, and fluorescence emission was measured using the multidetection microplate reader.

2.9. LC–MS quantification of PDAL

The catalytic TKS reaction buffer was collected and analyzed using LC-IT-TOF-MS on an ESI time-of-flight mass spectrometer (Shimadzu, Kyoto, Japan). A methanol gradient (0%–100%) was used as the elution buffer for 80 min at 30°C, whereas nitrogen was used as the desolation gas and nebulizer in both the negative and positive ion modes. The negative and positive ion spectra were generated by scanning in the range of 100–2,000 *m*/*z*.

2.10. Statistical analysis

Data are expressed as means ± standard deviation. Mean values between two groups were compared using Student's *t*-test, and $P < 0.05$ denoted a significant difference.

3. Results and discussion

3.1. Development of E. coli AraC variant-based PDAL biosensor

AraC is a regulatory protein that responds to $_L$-arabinose in *E. coli*. It regulates the gene transcription of the *ara* operon. When $_L$-arabinose is absent, the DNA-binding domains of AraC dimer bind to the I_1 and O_2 half-sites and repress transcription by forming a DNA loop upstream of the P_{BAD} promoter. However, when the N-terminal AraC arm binds to $_L$-arabinose, the AraC dimer changes conformation, such that the DNA-binding domains of AraC dimer bind to the I_1 and I_2 half-sites and activate the transcription by interacting with RNA polymerase at P_{BAD}. Thus, the dual regulatory property of AraC is dependent on a "light-switch" mechanism between the two conformations as well as on the interactions between the N-terminal domain amino acid residues and the effector. Point mutations in the N-terminal domain amino acid residues may change the ligand-binding pocket and alter molecular recognition in AraC. In this context, AraC responds to various small molecules [29]. In previous studies, AraC was engineered to respond to $_D$-arabinose, ectoine [34], mevalonate, and triacetic acid lactone [28]. In the present study, this previously reported platform was advanced for developing an AraC-based PDAL biosensor in *E. coli* (Fig. 2A). First, computational molecule docking and virtual screening programs were used to evaluate the interaction and binding energies of PDAL–AraC based on the structure of AraC- $_L$-arabinose (PDB: 2ARC). During the screening, the best-ranked mutants of Leu10Trp, Leu10Lys, Leu10Arg, Ile24Tyr, Ile24Trp, Ile24Phe, Ile24Lys, Ile24Glu, Ile24Gln, Ile36Lys, Ile36Glu, Ile36Gln, Ile36Arg, Arg38Tyr, Arg38Lys, Met42Trp, Met42Phe, Met42His, Met42Gln, Met42Arg, Phe15Lys, Phe15Arg, Ile36Trp, Ile36Phe, Ile36Tyr, Ile46Trp, Ile46Tyr, Ile46Phe, Arg93Lys, and Arg93Trp were considered potential positive mutants (Fig. S2). *E. coli* BL21 pET20b (+)-*araC*-P_{BAD}-*Kana* mutants containing the aforementioned screened variants were then assessed for their growth in LB medium containing 50 μg/mL ampicillin, 20 μg/mL kanamycin, 0.1 mM PDAL, and 0.1 mM IPTG. After culture for 12 h, six positive variants of Leu10Trp, Leu10Lys, Leu10Arg, Ile36Lys, Ile36Phe, and Ile46Trp showed a higher growth rate than wild-type variants in the presence of exogenous 0.1 mM PDAL (Fig. 2B). The OD_{600} values of these variants were improved by 13.26% ± 0.07%, 33.02% ± 1.32%, 56.86% ± 8.22%, 12.10% ± 0.01%, 21.72% ± 0.12%, and 4.18% ± 0.05%, respectively, compared with the control WT-AraC. Besides, PDAL was not consumed during the growth of *E. coli* BL21 pET20b (+) (Fig. 2C). Thus, PDAL was an effector for these AraC mutant strains. Moreover, PDAL activated the expression of ampicillin under the control of the pBAD promoter. These positive variants were considered candidates for exploring the dose–response profiles of PDAL using the AraC biosensor.

3.2. Characterization of AraC mutant biosensor response to PDAL

To explore the dose–response profiles of PDAL on the AraC biosensor, three *E. coli* BL21 pET20b (+)-*araC*-P_{BAD}-*gfp* mutants (Leu10Trp, Leu10Lys, and Leu10Arg) were established and cultured in LB broth containing 50 μg/mL ampicillin and 0.1 mM IPTG. The effect of exogenous PDAL concentration on GFP expression under the control of the promoter P_{BAD} and AraC mutant strain growth is shown in Fig. 3. *E. coli* growth was reduced when PDAL concentrations exceeded 0.8 mM, making PDAL quantification based on OD_{600} difficult for a saturating exogenous PDAL dose (Fig. 3A). However, GFP fluorescence increased as a function of PDAL concentration in a manner approximated by a Hill function, an observation that was similar to that for IPTG concentration [35]. Mathematical models for predicting PDAL concentrations and

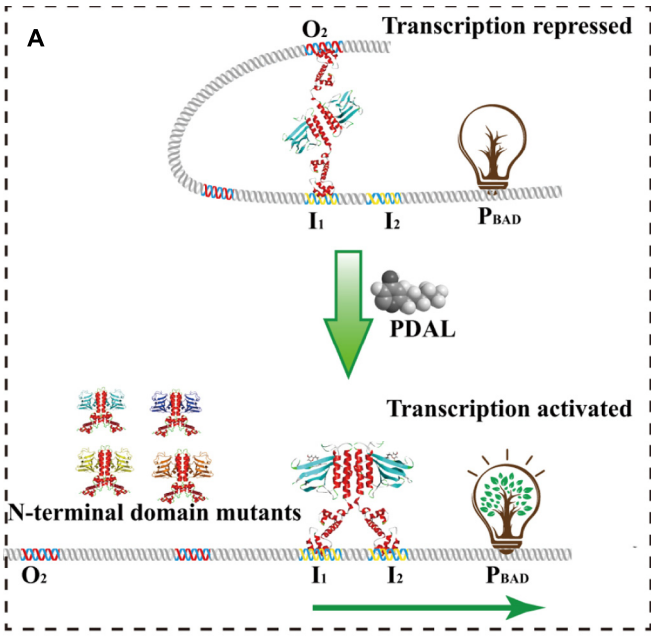

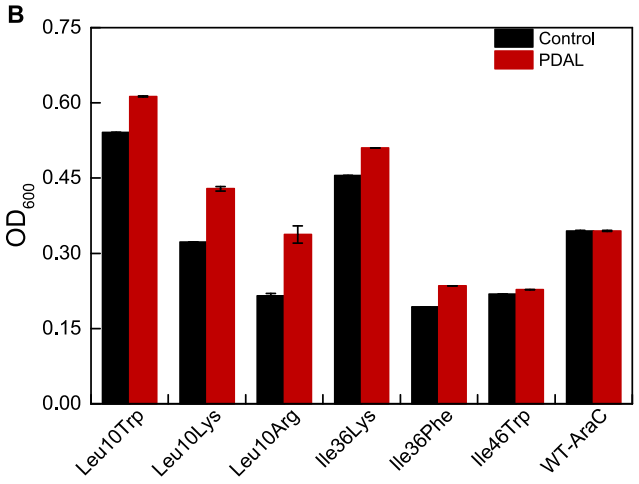

Fig. 2. Schematic diagram of the constructed AraC-based biosensors in *Escherichia coli* for PDAL assay. (A) Mechanism of dual regulation by AraC under the P_{BAD} promoter; I1, I2, and O_2 represent the DNA binding half-sites for the AraC DNA-binding domain (red color); (B) effect of PDAL on the growth of *E. coli* BL21 pET20b-*araC*-P_{BAD}-*Kana* mutants at 37°C with 220-rpm shaking. (C) Concentration of PDAL during the growth process of *Escherichia coli* BL21 pET20b (+).

GFP expression levels were fitted to Hill functions as follows: $y_{Leu10Arg} = 0.99789 + 0.64258 * x^{0.468}/(1.03732 + x^{0.468})$, $y_{Leu10Lys} = 0.98721 + 0.36097 * x^{0.468}/(1.03732 + x^{0.468})$, and $y_{Leu10Trp} = 0.99979 + 0.06426 * x^{0.468}/(1.03732 + x^{0.468})$ (Fig. 3B). The highest normalized GFP fluorescence values were 1.6407, 1.3842, and 1.0641, respectively. The mathematical models increased the objectivity and reliability of the PDAL concentration and GFP fluorescence assessments and predictions. This indicated that the expression response of the AraC (Leu10Arg)–PDAL reporter was relatively more specific to PDAL than to AraC (Leu10Trp)–PDAL and AraC (Leu10Lys)–PDAL reporters. For a detailed understanding of the molecular basis for improving the expression response of the AraC–PDAL reporter, a homology-based model of AraC–PDAL and its mutants AraC (Leu10Arg)–PDAL, AraC (Leu10Trp)–PDAL, and AraC (Leu10Lys)–PDAL was constructed. 10Leu was located on the gating loop ^{7}DPLLPGYSFNAHL^{19} in the substrate-binding pocket, which dictated the pocket's entrance width and thus con-

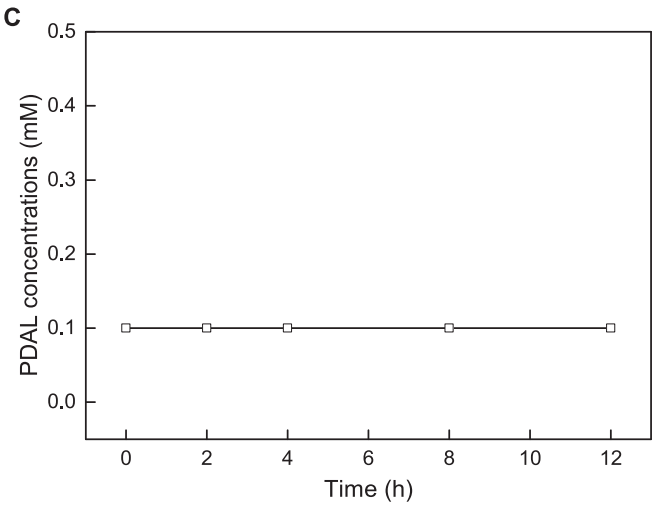

Fig. 2 (*continued*)

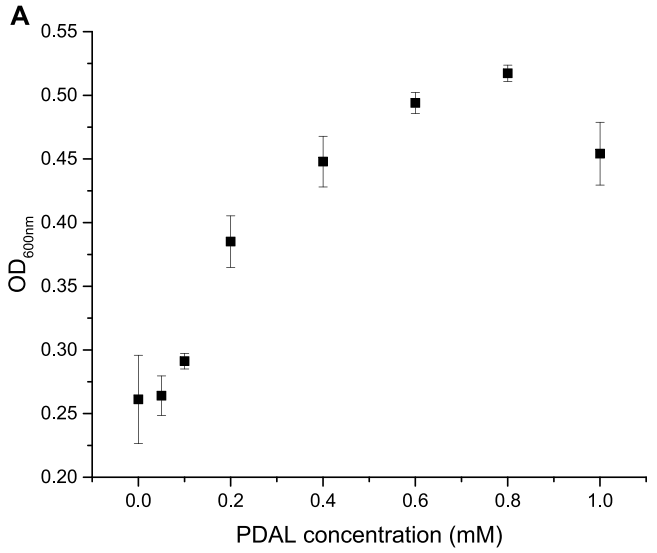

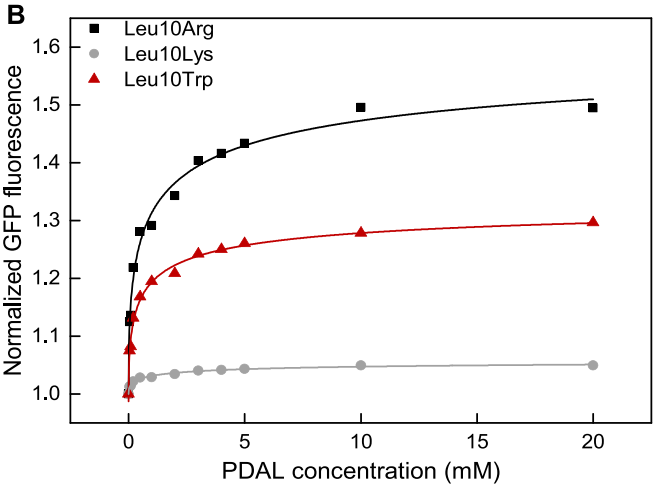

Fig. 3. AraC–PDAL PDAL dose response. (A) Effect of PDAL on the growth of *Escherichia coli*; (B) GFP expression in *E. coli* BL21 pET20b-*araC*-P_{BAD}-*gfp* mutant as a function of PDAL concentration; Leu10Arg, Leu10Lys, and Leu10Trp.

trolled PDAL entry and release. When 10Leu was mutated to the basic amino acids Arg, Lys, and Trp, the residues occupied the PDAL-binding pocket. The pocket bottleneck width for AraC was represented by the distance between the two points associated with the sidechains of residues 10 and 34 after AraC was bound to the PDAL substrates (Fig. S3). This enhanced the steric hindrance among the residues in the pocket, depressed the mobility of PDAL, and prevented PDAL from releasing, leading to a slightly larger affinity between AraC and PDAL.

3.3. In vitro PDAL assay in presence of TKS pathway

To determine *in vitro* PDAL concentration in the presence of the TKS pathway, the effect of the substrates and products of TKS catalysis on the growth rate, i.e., OD_{600}, of *E. coli* BL21 pET20b (+)-*araC* (Leu10Arg)-P_{BAD}-*Kana* was tested in the presence or absence of substrates and products. No activation in the strain growth was observed after *E. coli* BL21 pET20b (+)-*araC*-P_{BAD}-*Kana* was cultured at 37°C for 12 h in the presence of malonyl-CoA (substrate), hexanoyl-CoA (substrate), Hexanoyl triacetic acid lactone (product), olivetol (product), or Olivetolic acid (product) (Fig. 4A). Thus, the AraC-mutant biosensor did not respond to substrates and products. Indeed, the strain growth was reduced by 72% when the olivetol concentration was 0.8 mM. However, all these compounds had no effect on the GFP expression level of *E. coli* BL21 pET20b (+)-*araC* (Leu10Arg)-P_{BAD}-*gfp*. In this case, *E. coli* BL21 pET20b (+)-*araC* (Leu10Arg)-P_{BAD}-*gfp* was first cultured in 2*LB broth, induced by IPTG, and subsequently exposed to enzymatic blends at 10°C for 24 h to assess GFP fluorescence. Compared with the control, in which *E. coli* BL21 pET20b (+)-*araC* (Leu10Arg)-P_{BAD}-*gfp* was cultured without enzymatic blends, the normalized GFP fluorescence was 1.0969 ± 0.0033 and the corresponding PDAL concentration was 0.03 mM according to $y_{\mathrm{Leu10Arg}} = 0.99789 + 0.64258 * x^{0.468}/(1.03732 + x^{0.468})$, which was in agreement with the PDAL concentration detected via LC–MS (Fig. 4B).

3.4. In vivo PDAL detection in microbial fermentation

To determine *in vivo* PDAL concentration in microbial culture, the offline forms that assay the products and byproducts of enzymatic steps are not practical. The addition of the substrates malonyl-CoA and hexanoyl-CoA are required after cell disruption, which is time-consuming, labor-intensive, and expensive. To address this challenge, a PKS-producing strain of *E. coli* pCold-*TKS* was established that could catalyze the endogenous substrates malonyl-CoA and hexanoyl-CoA into different products. To determine the *in vivo* PDAL concentration, recombinant *E. coli* BL21 strain harboring pCold-*PKS* and pET20b (+)-*araC*(Leu10Arg)-P_{BAD}-*gfp*, *E. coli* BL21 strain harboring pCold-*PKS* and pET20b (+)-*araC* (Leu10Trp)-P_{BAD}-*gfp*, and *E. coli* BL21 strain harboring pCold-*PKS* and pET20b (+)-*araC*(Leu10Lys)-P_{BAD}-*gfp* were constructed. The time course of GFP fluorescence was recorded after IPTG was added to the broth. After 24-h culture, the normalized GFP fluorescence of the aforementioned recombinant strains was 1.1695 ± 0.0135, 1.10301 ± 0.0142, and 1.0172 ± 0.0023, respectively, compared with the GFP fluorescence of *E. coli* pCold-*TK*. Thus, the concentration of *E. coli* pCold-*TKS*-produced PDAL was 0.13 mM according to the following Hill functions:$y_{\mathrm{Leu10Arg}} = 0.99789 + 0.64258 * x^{0.468}/(1.03732 + x^{0.468})$, $y_{\mathrm{Leu10Lys}} = 0.98721 + 0.36097 * x^{0.468}/(1.03732 + x^{0.468})$, and $y_{\mathrm{Leu10Trp}} = 0.99979 + 0.06426 * x^{0.468}/(1.03732 + x^{0.468})$, in line with the PDAL concentration detected using LC–MS (Fig. 5).

In summary, a robust *E. coli* biosensor for detecting microbially produced PDAL was constructed using the rational engineering of

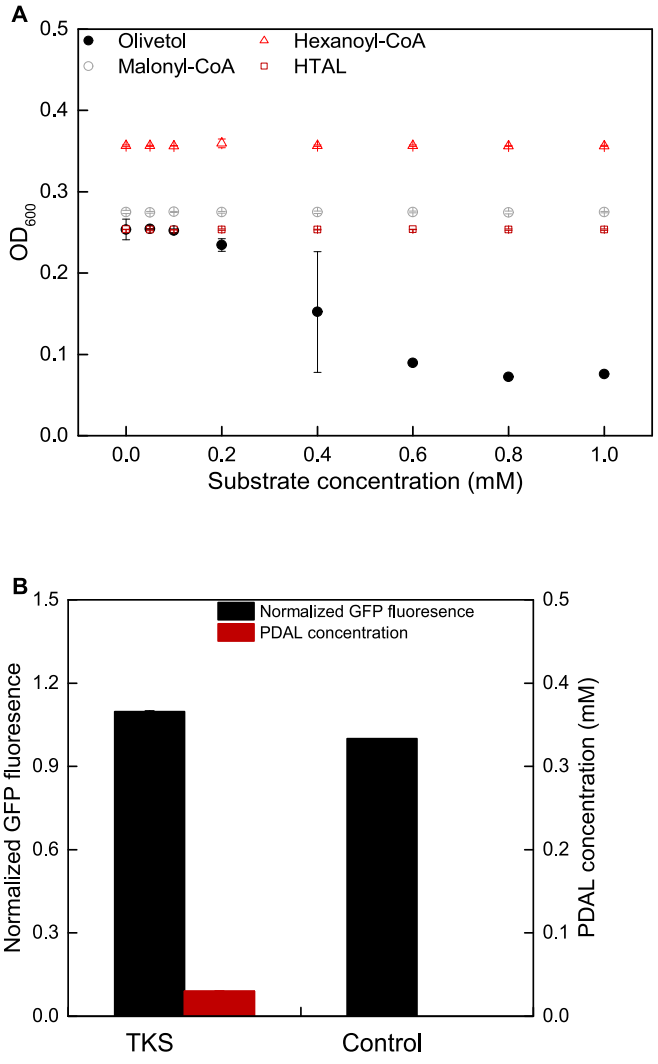

Fig. 4. *In vitro* PDAL concentration assay using *Escherichia coli* biosensor. (A) Effect of olivetol on the growth of *E. coli*; (B) PDAL concentration assay in the presence of the products of TKS catalysis.

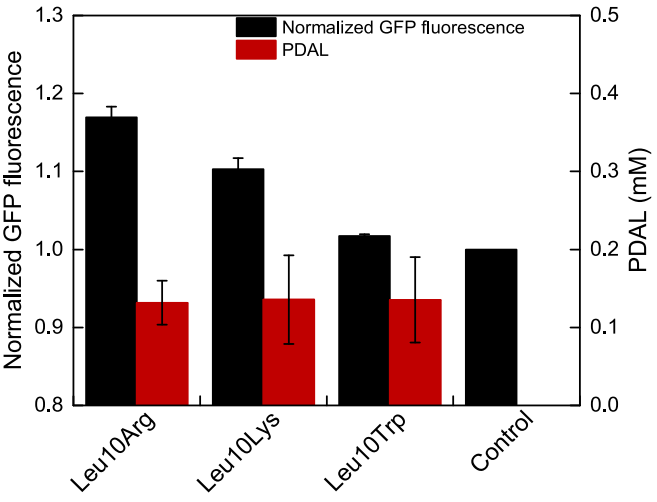

Fig. 5. Determination of PDAL concentration in microbial fermentation.

AraC N-terminal domain based on the structural design approach. The study results indicated that residues located on the N-terminal domain played a crucial role in the binding activity of AraC with different effectors. The AraC variants Leu10Trp, Leu10Lys, Leu10Arg, Ile36Lys, Ile36Phe, and Ile46Trp were responsive to PDAL and regulated the gene transcription under the P_{BAD} promoter. The present study results indicated that an AraC-based biosensor in *E. coli* was a cheap and powerful tool for PDAL assay both *in vivo* and *in vitro*, with potential applications in TKS engineering and cannabinoid bioproduct detection.

Author contributions

- Study conception and design: M Gao; Y Zhang; ZX Zhou.
- Data collection: M Gao; Y Zhang; Z Zhou; L Xue.
- Analysis and interpretation of results: J Li; XD Li; ZX Zhou.
- Draft manuscript preparation: M Gao; ZX Zhou.
- Revision of the results and approval of the final version of the manuscript: ZX Zhou; R Wang.

Financial support

This work was funded by the Natural Science Foundation of Jiangsu Province (BK20200293); the National Natural Science Foundation of China (Grant nos. 32071531, 32000068); the Open Fund of Jiangsu Key Laboratory for the Research and Utilization of Plant Resources (JSPKLB202201, JSPKLB202213, JSPKLB202026); the "333 project" of Jiangsu Province (Grant No. BRA2020082).

Conflict of interest

The authors declare no conflict of interest.

Data availability

Several files of the experimental assays carried out are provided in the supplementary material.

Supplementary material

Supplementary data to this article can be found online at https://doi.org/10.1016/j.ejbt.2023.09.002.

References

[1] Tang XY, Eitel K, Kaysser L, et al. A two-step sulfation in antibiotic biosynthesis requires a type III polyketide synthase. Nat Chem Biol 2013;9(10):610–5. https://doi.org/10.1038/nchembio.1310. PMid: 23912167.
[2] Bisht R, Bhattacharyya A, Shrivastava A, et al. An overview of the medicinally important plant type III PKS derived polyketides. Front Plant Sci 2021;12:746908. https://doi.org/10.3389/fpls.2021.746908. PMid: 34721474.
[3] Nivina A, Paredes SH, Fraser HB, et al. GRINS: Genetic elements that recode assembly-line polyketide synthases and accelerate their diversification. Proc Natl Acad Sci USA 2021;118(26):. https://doi.org/10.1073/pnas.2100751118. PMid: 34162709e2100751118.
[4] Zhou YC, Tao WT, Qi Z, et al. Structural and mechanistic insights into chain release of the polyene PKS thioesterase domain. ACS Catal 2022;12(1):762–76. https://doi.org/10.1021/acscatal.1c04991.
[5] Brauer A, Zhou QQ, Grammbitter GLC, et al. Structural snapshots of the minimal PKS system responsible for octaketide biosynthesis. Nat Chem 2020;12(8):755–63. https://doi.org/10.1038/s41557-020-0491-7. PMid: 32632186.
[6] Sulpizio A, Crawford CEW, Koweek RS, et al. Probing the structure and function of acyl carrier proteins to unlock the strategic redesign of type II polyketide biosynthetic pathways. J Biol Chem 2021;296:100328. https://doi.org/10.1016/j.jbc.2021.100328. PMid: 33493513.
[7] Walker PD, Weir ANM, Willis CL, et al. Polyketide β-branching: Diversity, mechanism and selectivity. Nat Prod Rep 2021;38(4):723–56. https://doi.org/10.1039/D0NP00045K. PMid: 33057534.
[8] Guo DM, Wang HY, Zhang SM, et al. The type III polyketide synthase supergene family in plants: Complex evolutionary history and functional divergence. Plant J 2022;112(2):414–42. https://doi.org/10.1111/tpj.15953. PMid: 36004534.
[9] Wang XH, Gao BW, Nakashima Y, et al. Identification of a diarylpentanoid-producing polyketide synthase revealing an unusual biosynthetic pathway of 2-(2-phenylethyl)chromones in agarwood. Nat Commun 2022;13(1):348. https://doi.org/10.1038/s41467-022-27971-z. PMid: 35039506.
[10] Zargar A, Lal R, Valencia L, et al. Chemoinformatic-guided engineering of polyketide synthases. J Am Chem Soc 2020;142(22):9896–901. https://doi.org/10.1021/jacs.0c02549. PMid: 32412752.
[11] Helfrich EJN, Ueoka R, Chevrette MG, et al. Evolution of combinatorial diversity in trans-acyltransferase polyketide synthase assembly lines across bacteria. Nat Commun 2021;12(1):1422. https://doi.org/10.1038/s41467-021-21163-x. PMid: 33658492.
[12] Kalkreuter E, Bingham KS, Keeler AM, et al. Computationally-guided exchange of substrate selectivity motifs in a modular polyketide synthase acyltransferase. Nat Commun 2021;12(1):2193. https://doi.org/10.1038/s41467-021-22497-2. PMid: 33850151.
[13] He LM, Zhang R, Shen JD, et al. Improving the low-temperature properties of an exo-inulinase via the deletion of a loop fragment located in its catalytic pocket. Electron J Biotechnol 2022;55:1–8. https://doi.org/10.1016/j.ejbt.2021.09.004.
[14] Radwan MM, Chandra S, Gul S, et al. Cannabinoids, phenolics, terpenes and alkaloids of *Cannabis*. Molecules 2021;26(9):2774. https://doi.org/10.3390/molecules26092774. PMid: 34066753.
[15] Hryhorowicz S, Kaczmarek-Rys M, Zielinska A, et al. Endocannabinoid system as a promising therapeutic target in inflammatory bowel disease - a systematic review. Front Immunol 2021;12:790803. https://doi.org/10.3389/fimmu.2021.790803. PMid: 35003109.
[16] Sledzinski P, Zeyland J, Slomski R, et al. The current state and future perspectives of cannabinoids in cancer biology. Cancer Med 2018;7(3):765–75. https://doi.org/10.1002/cam4.1312. PMid: 29473338.
[17] Blasco-Benito S, Moreno E, Seijo-Vila M, et al. Therapeutic targeting of HER2-CB_2R heteromers in HER2-positive breast cancer. PNAS 2019;116(9):3863–72. https://doi.org/10.1073/pnas.1815034116. PMid: 30733293.
[18] Andradas C, Truong A, Byrne J, et al. The role of cannabinoids as anticancer agents in pediatric oncology. Cancers 2021;13(1):157. https://doi.org/10.3390/cancers13010157. PMid: 33466435.
[19] Marzęda P, Drozd M, Wróblewska-Łuczka P, et al. Cannabinoids and their derivatives in struggle against melanoma. Pharmacol Rep 2021;73(6):1485–96. https://doi.org/10.1007/s43440-021-00308-1. PMid: 34264513.
[20] Villalobos P, Chavez MI, Olguin Y, et al. The application of polymerized lipid vesicles as colorimetric biosensors for real-time detection of pathogens in drinking water. Electron J Biotechnol 2012;15(1). https://doi.org/10.2225/vol15-issue1-fulltext-5.
[21] Villalonga A, Sanchez A, Mayol B, et al. Electrochemical biosensors for food bioprocess monitoring. Curr Opin Food Sci 2022;43:18–26. https://doi.org/10.1016/j.cofs.2021.09.006.
[22] Farina D, Zinellu M, Fanari M, et al. Development of a biosensor telemetry system for monitoring fermentation in craft breweries. Food Chem 2017;218:479–86. https://doi.org/10.1016/j.foodchem.2016.09.092 PMid: 27719939.
[23] Ejeian F, Etedali P, Mansouri-Tehrani H-A, et al. Biosensors for wastewater monitoring: A review. Biosens Bioelectron 2018;118:66–79. https://doi.org/10.1016/j.bios.2018.07.019 PMid: 30056302.
[24] Gavrilas S, Ursachi CS, Perta-Crisan S, et al. Recent trends in biosensors for environmental quality monitoring. Sensors 2022;22(4):1513. https://doi.org/10.3390/s22041513. PMid: 35214408.
[25] Eyvazi S, Baradaran B, Mokhtarzadeh A, et al. Recent advances on development of portable biosensors for monitoring of biological contaminants in foods. Trends Food Sci Tech 2021;114:712–21. https://doi.org/10.1016/j.tifs.2021.06.024.
[26] Abid SA, Muneer AA, Al-Kadmy IMS, et al. Biosensors as a future diagnostic approach for COVID-19. Life Sci 2021;273:119117. https://doi.org/10.1016/j.lfs.2021.119117. PMid: 33508293.
[27] Tang S-Y, Cirino PC. Design and application of a mevalonate-responsive regulatory protein. Angew Chem Int Ed 2011;50(5):1084–6. https://doi.org/10.1002/anie.201006083. PMid: 21268200.
[28] Tang SY, Qian S, Akinterinwa O, et al. Screening for enhanced triacetic acid lactone production by recombinant *Escherichia coli* expressing a designed triacetic acid lactone reporter. J Am Chem Soc 2013;135(27):10099–103. https://doi.org/10.1021/ja402654z. PMid: 23786422.
[29] Tang S-Y, Fazelinia H, Cirino PC. AraC regulatory protein mutants with altered effector specificity. J Am Chem Soc 2008;130(15):5267–71. https://doi.org/10.1021/ja7109053. PMid: 18355019.
[30] Durrant JD, de Oliveira CAF, McCammon JA. POVME: An algorithm for measuring binding-pocket volumes. J Mol Graph Model 2011;29(5):773–6. https://doi.org/10.1016/j.jmgm.2010.10.007. PMid: 21147010.
[31] Fricke PM, Link T, Gatgens J, et al. A tunablel-arabinose-inducible expression plasmid for the acetic acid bacterium *Gluconobacter oxydans*. Appl Microbiol Biotechnol 2020;104(21):9267–82. https://doi.org/10.1007/s00253-020-10905-4. PMid: 32974745.
[32] Duarte JM, Barbier I, Schaerli Y. Bacterial microcolonies in gel beads for high-throughput screening of libraries in synthetic biology. ACS Synth Biol 2017;6(11):1988–95. https://doi.org/10.1021/acssynbio.7b00111. PMid: 28803463.

[33] Gagne SJ, Stout JM, Liu E, et al. Identification of olivetolic acid cyclase from *Cannabis sativa* reveals a unique catalytic route to plant polyketides. Proc Natl Acad Sci USA 2012;109(31):12811–6. https://doi.org/10.1073/pnas.1200330109. PMid: 22802619.
[34] Chen W, Zhang S, Jiang P, et al. Design of an ectoine-responsive AraC mutant and its application in metabolic engineering of ectoine biosynthesis. Metab Eng 2015;30:149–55. https://doi.org/10.1016/j.ymben.2015.05.004 PMid: 26051748.
[35] Castillo-Hair SM, Fujita M, Igoshin OA, et al. An engineered *B. subtilis* inducible promoter system with over 10 000-fold dynamic range. ACS Synth Biol 2019;8(7):1673–8. https://doi.org/10.1021/acssynbio.8b00469. PMid: 31181163.